

TractSeg - Fast and accurate white matter tract segmentation

Jakob Wasserthal ^{a,b}, Peter Neher ^a, Klaus H. Maier-Hein ^{a,c}

^a Division of Medical Image Computing (MIC), German Cancer Research Center (DKFZ), Heidelberg, Germany

^b Medical Faculty Heidelberg, University of Heidelberg, Heidelberg, Germany

^c Section for Automated Image Analysis, Heidelberg University Hospital, Heidelberg, Germany
{j.wasserthal, p.neher, k.maier-hein}@dkfz.de

Abstract. The individual course of white matter fiber tracts is an important key for analysis of white matter characteristics in healthy and diseased brains. Uniquely, diffusion-weighted MRI tractography in combination with region-based or clustering-based selection of streamlines allows for the in-vivo delineation and analysis of anatomically well known tracts. This, however, currently requires complex, computationally intensive and tedious-to-set-up processing pipelines. TractSeg is a novel convolutional neural network-based approach that directly segments tracts in the field of fiber orientation distribution function (fODF) peaks without requiring tractography, image registration or parcellation. We demonstrate in 105 subjects from the Human Connectome Project that the proposed approach is much faster than existing methods while providing unprecedented accuracy. The code and data are openly available at <https://github.com/MIC-DKFZ/TractSeg/> and <https://doi.org/10.5281/zenodo.1088277>, respectively.

1. Introduction

White matter fiber tract segmentation enables detailed analysis of individual white matter tracts. It helps to characterise the healthy brain and identify areas containing abnormal morphology in diseased brains (Bells et al., 2011, Yendiki et al., 2011, Yeatman et al., 2012, Dayan et al., 2016). Such tractometry analyses are inherently dependent on the quality of the underlying tract segmentation, thus requiring accurate delineations.

Currently, the most commonly employed approach to segment white matter tracts is *virtual dissection*: streamlines that correspond to anatomically well-defined tracts are manually extracted from a tractogram using combinations of inclusion and exclusion regions-of-interest (ROIs) (Wang et al., 2007, Stieltjes et al., 2013, Thiebaut de Schotten et al., 2011). This is a very time consuming process that has a limited reproducibility due to the subjectivity in the human interaction. Therefore, a variety of automatic approaches for white matter segmentation have been proposed. They can be grouped into three categories: *ROI-based segmentation*, *clustering-based segmentation* and *direct segmentation*.

ROI-based segmentation approaches typically employ information from a common atlas space that is registered to the subject in order to extract ROIs in the cortex (parcellation) or in the white matter. Streamlines are then filtered according to their spatial relation to these ROIs (Cook et al., 2005).

This is a preprint of a journal submission currently under review.

© 2018. This manuscript version is made available under the CC-BY-NC-ND 4.0 license

Yendiki et al. (2011) use a white matter atlas to specify the morphology of tracts. Wassermann et al. (2016) use a Freesurfer parcellation to characterize different tracts. Yeatman et al. (2012) use a probabilistic atlas.

Clustering-based segmentation approaches group streamlines into anatomically (Siless et al., 2018) or spatially coherent clusters. These clusters are either manually (O'Donnell et al., 2016) or automatically, e.g. using prior knowledge in form of a white matter (WM) atlas, assigned to anatomically meaningful fiber tracts (Jin et al., 2014). Garyfallidis et al. proposed an alternative approach where the white matter atlas is replaced by a streamline atlas that can be directly incorporated into the clustering process (Garyfallidis et al., 2017, Labra et al., 2017). Clayden et al. also uses reference tracts combined with a tract similarity measure to segment tracts (Clayden et al., 2007, Clayden et al., 2009).

ROI- and clustering-based methods involve whole series of processing steps for atlas registration, tractography, parcellation or clustering. The resulting pipelines are rather complex, computationally expensive and tedious to fine-tune. For example, most methods base their inter-subject consistency on a registration between subject and atlas. This in itself is a non trivial task that requires quality checking and that might introduce subtle errors which are then propagated through all further processing steps.

Direct segmentation approaches circumvent the intermediate generation of streamlines, thus simplifying the processing chain by directly producing complete tract segmentations from the input images. A variety of direct methods has already been presented, employing techniques like template matching (Eckstein et al., 2009), markov random field optimization (Bazin et al., 2011), geometric flow-based segmentation (Guo et al., 2008, Jonasson et al., 2005), surface evolution (Lenglet et al., 2006) and k-NN based classification (Ratnarajah et al., 2014). However, most of the available direct segmentation methods show incomplete segmentations, making recent research focus on ROI- and clustering-based approaches.

We propose TractSeg as a novel approach to direct white matter tract segmentation that provides complete and accurate segmentations, yet is easy to set up, fast to run and does not require registration, parcellation, tractography or clustering. This is achieved by a fully convolutional neural network (FCNN) that directly segments white matter tracts in fields of fiber orientation distribution function (fODF) peaks. We demonstrate the efficacy of our approach by segmenting a total of 72 anatomically well-described tracts in a cohort of 105 subjects selected from the Human Connectome Project (HCP) (Van Essen et al., 2013), comparing to six other state of the art tract segmentation methods.

2. Materials and Methods

The core of our method is an encoder-decoder FCNN that processes the data and generates tract probability maps. Figure 1 gives an overview of the proposed segmentation workflow.

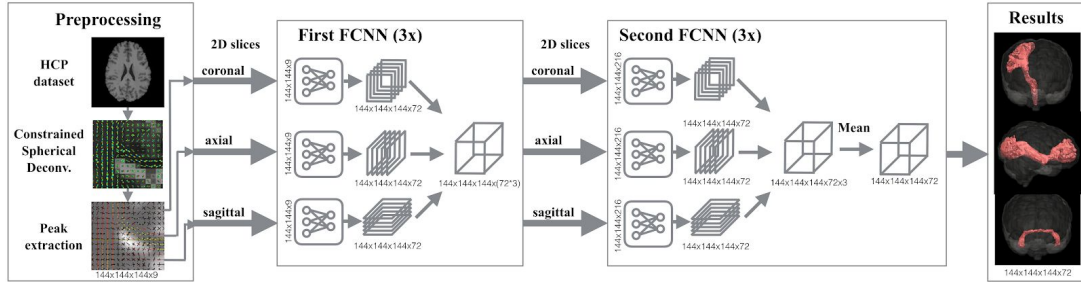


Figure 1: TractSeg segmentation pipeline. Constrained Spherical Deconvolution is used to extract the three dominant diffusion directions in each voxel. A 2D encoder-decoder FCNN then produces one tract probability image stack for each orientation (coronal, axial, sagittal) and for each tract. To generate final tract segmentations, the tract probability image stacks are concatenated and used as input for a second FCNN which again runs three times. The three outputs per tract from the second FCNN are merged using the *Mean* to generate the final segmentation.

2.1. Preprocessing

While raw image values could have been used as input for our method, this would restrict the method to the used MRI acquisition, not even allowing slight variations in the acquisition setup without a complete retraining of the method. Moreover, for high angular resolution datasets it would result in an input image with a huge number of channels, creating high memory demand and slow file input/output during training. A more condensed representation of the data was chosen to mitigate this problem: TractSeg expects the three principal fiber directions per voxel as input, thus requiring nine different input channels (three per principal direction). In this study, the principal directions were extracted using the multi-shell multi-tissue constrained spherical deconvolution (CSD) and peak extraction available in MRtrix (Jeurissen et al., 2014, Tournier et al., 2007) with a maximum number of three peaks per voxel.

2.2. Convolutional Neural Network

The proposed 2D encoder-decoder FCNN architecture was inspired by the U-Net encoder-decoder architecture previously proposed by Ronneberger et al. (Ronneberger et al., 2015). Figure 2 details the proposed network setup.

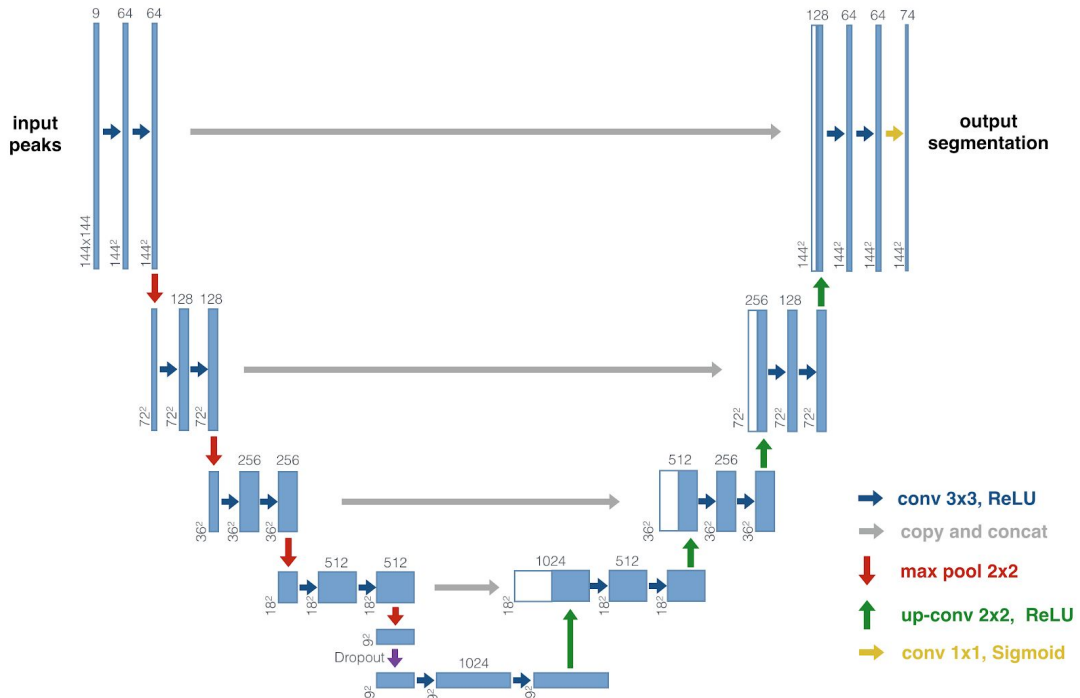


Figure 2: Proposed TractSeg FCNN architecture. Blue boxes represent multi-channel feature maps. White boxes show copied feature maps. The gray number on top of each box gives the number of channels, the x-y-size is given at lower left corner of each box. Network operations are represented by differently colored arrows.

The output of the proposed network is a multi-channel image, where each channel contains the voxel probabilities for one tract. The approach allows for multilabel segmentations with several tracts sharing one voxel. To enable this, the softmax activation in the last layer was replaced by a sigmoid activation, which does not require the probabilities of all classes to sum to one. To avoid a downsized output in comparison to the input we padded with half the filter size (rounded down) on both sides. This is also referred to as SAME padding (Dumoulin et al., 2016).

While the U-Net architecture in principle allows extensions to 3D image segmentation (Çiçek et al., 2016), we propose using 2D slices as input to be more memory efficient and able to process the data at the original high resolution. To still leverage the additional information provided by the third dimension, we randomly sampled 2D slices in three different directions during training: axial, coronal and sagittal. This way our model learned to work with all three of these directions. During inference three predictions per voxel were generated, one for each orientation. A second FCNN with three input channels was trained to optimally fuse the three predictions per voxel into one final segmentation. TractSeg was thus able to learn individually for each tract or part of tract which combination of slice orientations yields the best prediction. The second FCNN was also trained on 2D slices sampled randomly from axial, coronal and sagittal directions. Similar to the first FCNN the second FCNN was as well used to generate three predictions per voxel during inference. The final prediction was then produced by mean aggregation.

2.3. Training

We trained our network using the binary cross-entropy loss. For a given target t , an output of the network o and n number of classes the loss was calculated as

$$\text{loss}(o, t) = -\frac{1}{n} \sum_{i=0}^n (t[i] * \log(o[i]) + (1 - t[i]) * \log(1 - o[i])).$$

As nonlinearity we used rectified linear units (ReLU) (Nair and Hinton, 2010). Only in the last layer sigmoid activation functions were used. Sigmoid activation paired with binary cross-entropy enables multilabel segmentations. A learning rate of 0.002 was used und Adamax (Kingma and Ba, 2014) as optimizer. The batch size was 56. We used dropout (Srivastava et al., 2014) with a probability of 0.4 and trained for 500 epochs. All hyperparameters were optimized on a validation dataset independent of the final test dataset. The network weights of the epoch with the highest Dice score during validation were used for testing.

To improve the generalizability of TractSeg we applied heavy data augmentation during training¹. To each training sample the following transformations were applied. The intensity of each transformation was varied randomly.

- Rotation by angle $\phi_x \sim U[-\pi/4, \pi/4]$, $\phi_y \sim U[-\pi/4, \pi/4]$, $\phi_z \sim U[-\pi/4, \pi/4]$
- Elastic deformation with alpha and sigma $(\alpha, \sigma) \sim (U[90, 120], U[9, 11])$. For each voxel a displacement vector is sampled $d \sim U[-1, 1]$, which is then smoothed by a gaussian filter with standard deviation σ and finally scaled by α .
- Displacement by $(\Delta x, \Delta y) \sim (U[-10, 10], U[-10, 10])$
- Zooming by a factor $\lambda \sim U[0.9, 1.5]$
- Resampling (to simulate lower image resolution) with factor $\lambda \sim U[0.5, 1]$
- Gaussian Noise with mean and variance $(\mu, \sigma) \sim (0, U[0.05])$
- Contrast augmentation $X_{augmented} = (X - \text{avg}(X)) * \beta + \text{avg}(X)$ with $\beta \sim U[0.7, 1.3]$
- Brightness augmentation $X_{augmented} = X * \gamma$ with $\gamma \sim U[0.7, 1.3]$

The results presented in section 3 were obtained with an implementation of the proposed method in Lasagne (Dieleman et al., 2015). Additionally we provide a Pytorch (pytorch.org) implementation.

2.4. Reference Segmentations

For all experiments 105 subjects from the Human Connectome Project were used. The corresponding dMRI images have 1.25mm isotropic resolution and 270 gradient directions with 3 b-values (1000, 2000, 3000 s/mm²) and 18 b=0 images (Sotiropoulos et al., 2013). We semi-automatically generated reference segmentations for 72 major white matter tracts for each subject (figure 3) using a series of 5 processing steps (figure 4):

¹ <https://github.com/MIC-DKFZ/batchgenerators>

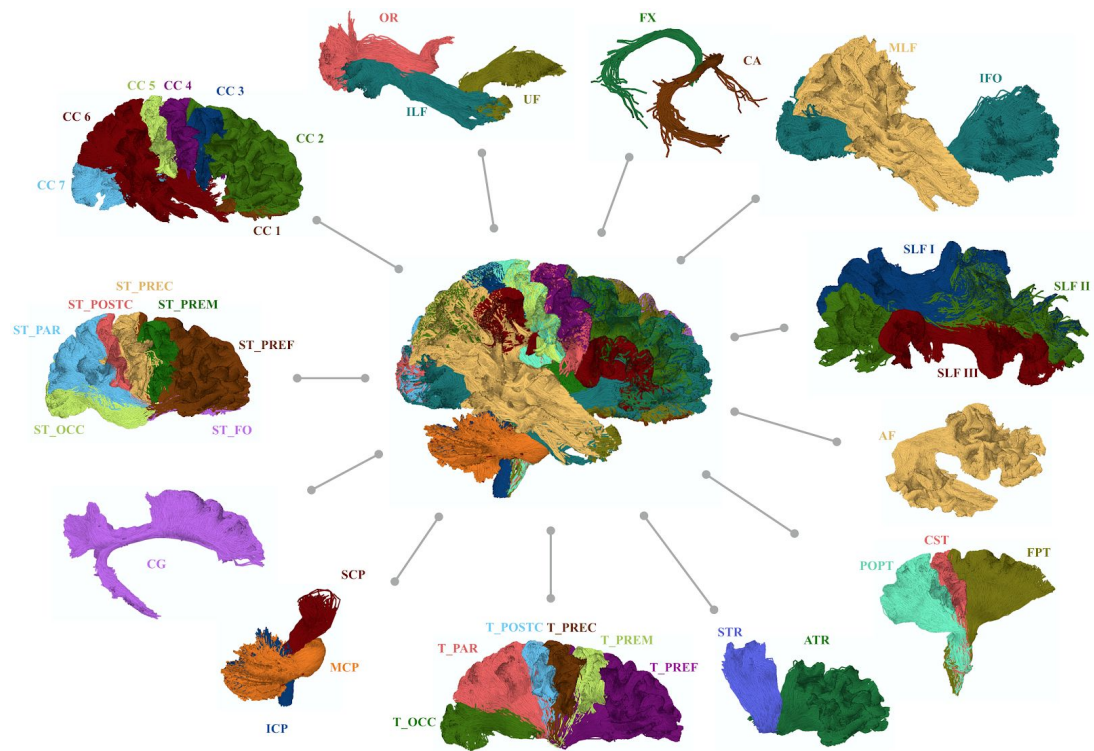


Figure 3: Overview of all 72 tracts. For tracts which exist in the left and the right hemisphere only the right one is shown. The following tracts are included: Arcuate fascicle (AF), Anterior thalamic radiation (ATR), Commissure anterior (CA), Corpus callosum (Rostrum (CC 1), Genu (CC 2), Rostral body (CC 3), Anterior midbody (CC 4), Posterior midbody (CC 5), Isthmus (CC 6), Splenium (CC 7)), Cingulum (CG), Corticospinal tract (CST), Middle longitudinal fascicle (MLF), Fronto-pontine tract (FPT), Fornix (FX), Inferior cerebellar peduncle (ICP), Inferior occipito-frontal fascicle (IFO), Inferior longitudinal fascicle (ILF), Middle cerebellar peduncle (MCP), Optic radiation (OR), Parieto-occipital pontine (POPT), Superior cerebellar peduncle (SCP), Superior longitudinal fascicle I (SLF I), Superior longitudinal fascicle II (SLF II), Superior longitudinal fascicle III (SLF III), Superior thalamic radiation (STR), Uncinate fascicle (UF), Thalamo-prefrontal (T_PREF), Thalamo-premotor (T_PREM), Thalamo-precentral (T_PREC), Thalamo-postcentral (T_POSTC), Thalamo-parietal (T_PAR), Thalamo-occipital (T_OCC), Striato-fronto-orbital (ST_FO), Striato-prefrontal (ST_PREF), Striato-premotor (ST_PREM), Striato-precentral (ST_PREC), Striato-postcentral (ST_POSTC), Striato-parietal (ST_PAR), Striato-occipital (ST_OCC)

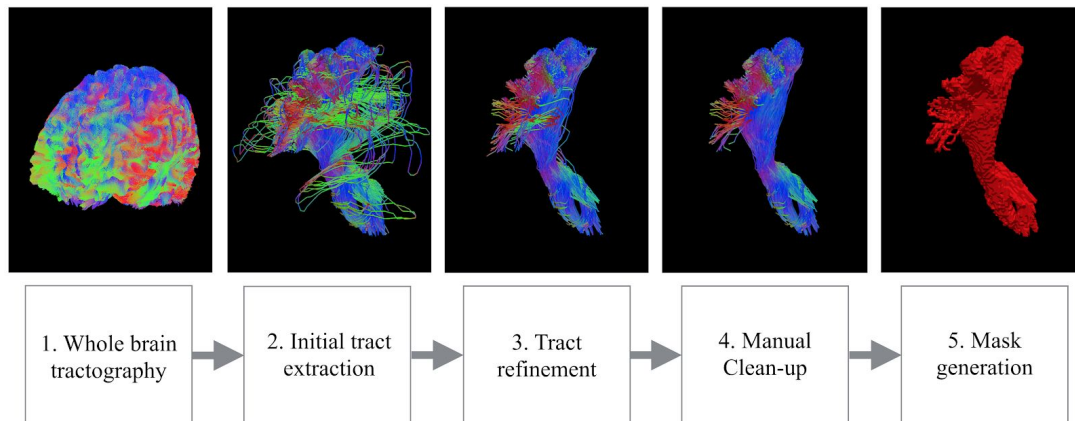


Figure 4: Exemplary depiction of the semi-automatic dissection pipeline of a total of 72 reference tracts in a cohort of 105 subjects. Images show the left CST of subject 898176.

Step 1 - Tractography. Multi-shell multi-tissue constrained spherical deconvolution was used to extract the fODF and anatomically constrained probabilistic tractography (iFOD2) was performed using MRtrix (Tournier et al., 2010) to generate 10 million fibers with a minimum length of 40mm. By generating such a large number of fibers we were able to reconstruct difficult tracts like the anterior commissure (CA) or the lateral projections of the corticospinal tract (CST) with high completeness in the majority of subjects. Extracting fibers that run completely from the left cortex through the CA to the right cortex is difficult if using a smaller number of fibers. The high fiber count however comes at the cost of many false positives which we eliminated in the next steps. Seeds were randomly placed within the brain mask. Streamlines were cropped at the gray-matter-white-matter interface.

Anatomically constrained tractography yielded adequate results for the majority of tracts. However, for tracts containing very thin parts like the CA, uncinate fascicle (UF) or inferior occipito-frontal fascicle (IFO) the anatomical constraints did not work well. They are based on a gray matter segmentation which is based on the T1 image and does not necessarily fit perfectly to the diffusion weighted image. If a tract is only a few voxels wide and the gray matter segmentation is not perfect, some critical parts of the tract will be cut off because they are counted as gray matter. Therefore we used tracking without anatomical constraints for CA, UF and IFO.

Step 2 - Initial tract extraction. To extract a first approximation of each tract and to make sure streamlines end in the correct cortex regions we applied TractQuerier (Wassermann et al., 2016). Our queries are based on the queries provided by Wassermann et al. (2016) with minor adaptations for better results with our dataset. The queries used in this work are available online².

Step 3 - Tract refinement. The results of TractQuerier contained a considerable amount of false positives (see figure 4). So further filtering was needed. We manually defined exclusion and inclusion ROIs to clear out false positives (Stieltjes et al., 2013). These ROIs were transferred between subjects using diffeomorphic registration of the fractional anisotropy (FA) maps.

We further removed streamlines that run back and forth in the target volume, i.e. making 180 degree turns within less than 30 mm distance. More spurious fibers were filtered by running QuickBundles clustering (Garyfallidis et al., 2012) and removing clusters that contain only a small number of fibers

² https://github.com/MIC-DKFZ/TractSeg/blob/master/examples/WMQL_Queries.qry

according to varying thresholds for each tract. This approach was only used in a very cautious way as it tends to remove also valid parts like the lateral projects of the CST, which are rather sparse in streamline space and therefore typically consists of small clusters. Finally, we removed all streamlines that run through voxels with low streamline density (threshold differs for each tract).

Step 4 - Manual quality control, clean-up. The described steps for automated tract refinement occasionally removed some of the valid parts of a tract. We manually inspected the results of all filtering steps in all subjects and skipped some of the filters if they removed too many valid fibers. Having finished this process, there were still remaining streamlines that could only be filtered by manually drawing individual exclusion ROIs (Stieltjes et al., 2013). The UF for example tended to contain parts of the CA. Because of inaccurate Freesurfer parcellations those could not be properly excluded with TractQuerier in all subjects. The needed exclusion ROI had to be drawn very close to the valid part of the UF. Since it required a highly accurate placement, this ROI had to be manually drawn for each subject instead of using the same ROI for all subjects.

Step 5 - Mask Generation. This semi-automatic process resulted in high quality dissections of a total of 72 tracts in a cohort of 105 subjects. From the final sets of streamlines we created binary tract masks as reference segmentations used for training and testing of the proposed segmentation approach.

2.5. Reference methods

The following automatic tract segmentation methods were used as a benchmark. All these methods are openly available and do not need any proprietary software to run. The methods include clustering-based as well as ROI-based approaches. We roughly explain how they work (1.) and how we applied them (2.).

RecoBundles: 1. Given streamlines of a reference tract in a reference subject RecoBundles (Garyfallidis et al., 2017) can be used to find the corresponding streamlines in a new subject. 2. We randomly picked 5 reference subjects. Due to the long runtime of RecoBundles a higher number of reference subjects was not feasible. Then for a new subject we ran RecoBundles 5 times (once for each reference subject) using the default RecoBundles parameters. This resulted in 5 extractions of each tract in the new subject. To get a final segmentation we took the mean of those 5 extractions.

TRACULA: 1. TRACULA (Yendiki et al., 2011) uses probabilistic tracking and an atlas of the underlying anatomy to segment tracts. 2. Running TRACULA for each subject resulted in a probability map for each tract. We selected all voxels with probability greater than 0 to create a binary segmentation. The original paper created a binary segmentation by masking out all values below 20% of the maximum. However, this leaves only the very core of every tract, thus creating many false negatives. Segmenting all values with probability greater than 0 gives better results compared to our reference tracts. TRACULA does not support all 72 tracts we are using but only 18. Out of the 18 only 8 tracts exactly match tracts out of our 72. Therefore quantitative comparison was only performed on those 8 tracts. For *bedpostx* which is part of the TRACULA pipeline a GPU implementation is available which we used (Hernandez et al., 2013).

WhiteMatterAnalysis (WMA): 1. WMA (O'Donnell et al., 2012; O'Donnell and Westin, 2007) clusters streamlines across subjects and generates a cluster atlas out of those. Clusters in the atlas are then assigned to certain anatomical tracts. By registering new subjects to this atlas automated tract delineation is possible. 2. WMA comes with a pretrained cluster atlas (800 clusters) and a predefined mapping of clusters to anatomical tracts (O'Donnell et al., 2016). However, this mapping only includes 10 of the 72 tracts we use. We manually optimized these predefined mappings to better align it with our reference tracts and added the CA to the mapping. During this process, we were inherently limited by the finite set of distinct clusters offered by the atlas. We chose not to extend the mapping to the remaining 61 tracts as it would have required considerable manual effort given the amount of clusters and tracts. So evaluation was only done on these 11 tracts. WMA is very memory intensive. Clustering a tractogram with 1 million fibers needs around 60GB of memory. Therefore we were not able to directly use our 10 million fibers tractogram, but instead used a subset with only 500,000 fibers. This reduced the memory consumption to around 30GB. The outlier removal provided by WMA was used to remove spurious fibers.

TractQuerier: 1. TractQuerier (Wassermann et al., 2016) extracts tracts based on the regions the streamlines have to start in, end in and (not) run through. 2. We compared our method to the output from TractQuerier (step 2 from the reference tract extraction pipeline) without any further post-processing.

In addition to these openly available reference methods, we implemented two additional reference methods in order to provide further insights about the performance of TractSeg:

Atlas registration (Atlas): 1. Several subjects can be averaged to an atlas which can then be registered to new subjects to segment structures. 2. We split our data in training and testing data, using the same 5-fold cross-validation as used for evaluation our proposed method. The training data was used to create a tract atlas. Therefore we first registered all subjects to a random subject using symmetric diffeomorphic registration implemented in dipy (Avants et al., 2009). Registration was performed based on the FA maps of each image. After registration the FA maps of all images were averaged. Then in a second iteration all images were registered to this mean FA image. This two-stage approach limits the bias introduced by the initial subject choice in the first iteration. The tract atlas then contained the mean of the tract masks of each registered subject, thresholded at 0.5. During test time, the atlas was registered to the subjects of interest, yielding a binary mask for each tract in subject space.

Multiple mask registration (Multi-Mask): 1. Using an atlas can blur some of the details as it is based on group averages. The blurring can be reduced to some extent by registering the masks of single training subjects to a test subject instead of an averaged atlas. 2. The same 5 reference subjects as for RecoBundles were picked. To segment the tracts in a new subject we registered each of the 5 reference subjects to the new subject (symmetric diffeomorphic registration of the FA maps) and averaged the tract masks of all 5 reference subject. Finally we thresholded this average at 0.5 and got a binary mask for each tract in the space of the new subject.

There are more methods openly available for tract segmentation. However, setting up a reference method and evaluating it for all subjects and tracts includes considerable effort. Therefore we limited

our evaluation to 6 reference methods, covering a broad scope of approaches. Most other methods follow a somewhat similar approach to one of these.

3. Experiments and results

To extract the best possible reference tracts the high quality HCP data (*HCP Quality*) was used. However, in clinical routine faster MRI protocols are used which result in lower quality data. To test how TractSeg performs on clinical quality data, we downsampled the HCP data to 2.5mm isotropic resolution and removed all but 32 weighted volumes at $b=1000 \text{ s/mm}^2$. We call this dataset *Clinical Quality*. As this dataset only has one b-value shell, we can not use multi-shell CSD as we did for the *HCP Quality* data. Instead MRtrix standard CSD was employed to generate the peaks of the fODF. 5 fold cross validation was used, i.e. 63 training subjects, 21 validation subjects (best epoch selection) and 21 test subjects per fold. To test for statistical significance the Wilcoxon signed-rank test (Wilcoxon, 1945) was used. For multiple testing we applied the Bonferroni correction. Moreover, we evaluate the runtime of the different methods, the influence of different orientation fusion strategies and how TractSeg generalizes to non-HCP data.

3.1. Quantitative evaluation

On the *HCP Quality* data, TractSeg significantly ($p<0.001$) outperformed the second best method by 9 Dice points and on average performed 19 Dice points better than the other reference methods (figure 5a). On the *Clinical Quality* data, TractSeg significantly ($p<0.001$) outperformed the second best method by 14 Dice points and on average performed 22 Dice points better than the reference methods (figure 5b). In general, TractSeg was less affected by the quality loss in the clinical data than the reference methods. Please note that WMA and TRACULA provide segmentations only for a subset of the 72 tracts. The reported scores for WMA and TRACULA are restricted to this subset.

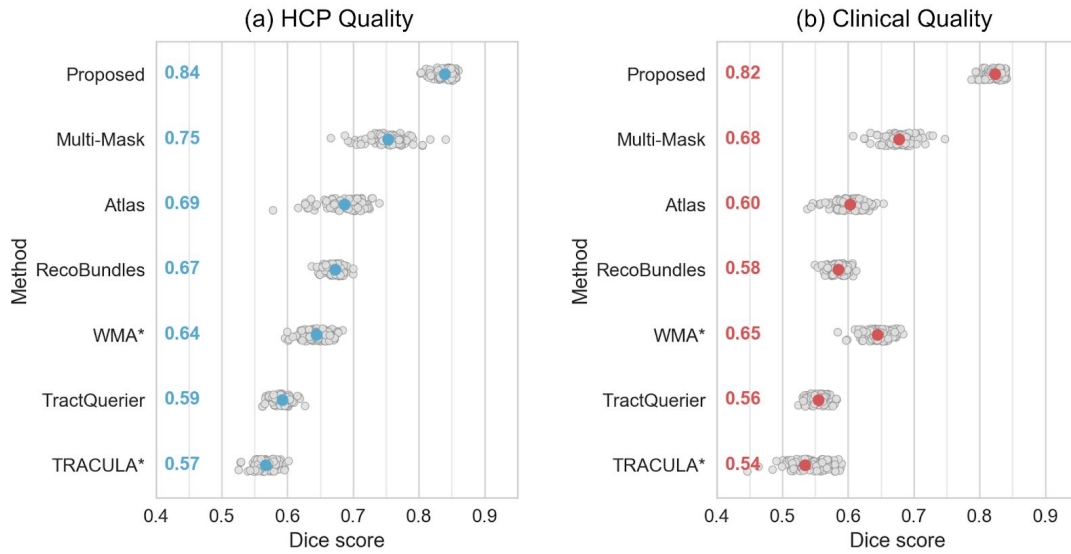


Figure 5: Results on (a) the *HCP Quality* dataset and (b) the *Clinical Quality* dataset with a gray dot per subject (mean over all tracts) and a colored dot for the mean over all subjects. *Proposed*: our method; *Multi-Mask*: Multiple mask registration; *Atlas*: Atlas registration; *WMA*: WhiteMatterAnalysis.

*: *WMA* and *TRACULA* do not provide segmentations for all tracts, but only for a subset. The score is the mean over the tracts in the subset.

Figure 6 shows the segmentation performance of all methods for each individual tract. TractSeg showed quite consistent performance. All tracts had a dice score over 0.75, except for the fornix (FX) and CA. For these two tracts, the Dice score was noticeably reduced, which is probably caused by the thin and therefore hard to reconstruct shape of these tracts. Moreover, due to limited sensitivity of the initial tractograms, in the reference tracts the CA and FX were not perfectly reconstructed for some subjects while our model managed to generate a segmentation better than the reference segmentation (see section 3.2). Therefore good segmentations also received bad Dice scores if the reference segmentation was flawed. The reference methods showed a similar accuracy gap between the FX and CA and the remaining tracts. Overall TractSeg clearly outperformed the reference methods.

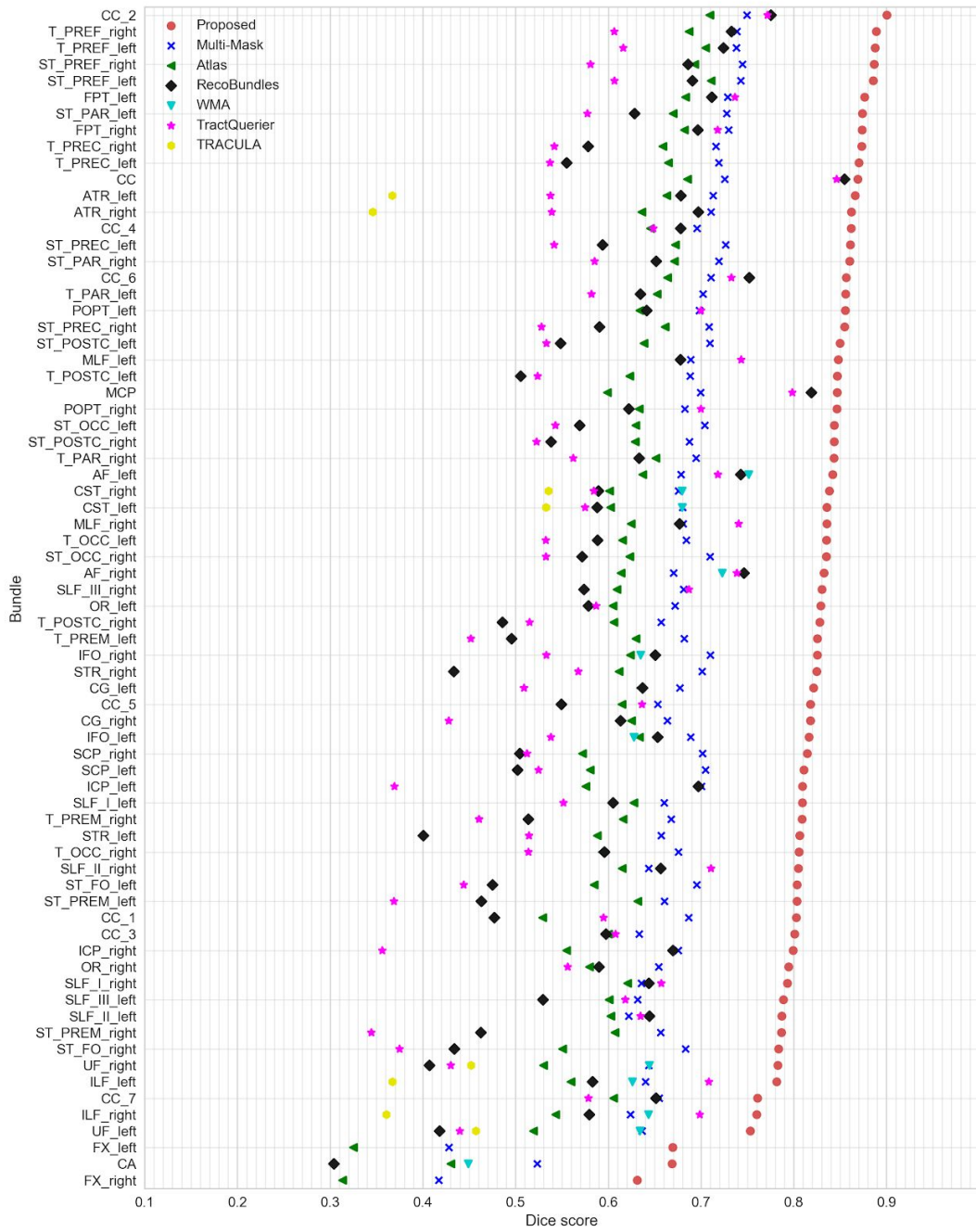


Figure 6: Dice scores for all 72 tracts on the *Clinical Quality* dataset for our proposed method and all reference methods sorted by score. The full name of each tract can be seen in figure 3.

3.2. Qualitative evaluation

For qualitative evaluation one subject (992774) was randomly selected from the test set. Since the scope of this manuscript does not allow to show results for all 72 tracts, we selected three tracts that are representative for different degrees of reconstruction difficulty (Maier-Hein et al., 2017): IFO, CST and CA (results for all tracts can be accessed online³). The IFO is a fairly easy to reconstruct tract, which is reflected by its consistently good scores for all methods. The CST is more difficult to reconstruct. The beginning at the brain stem is easy to reconstruct but as the fibers get closer to the cortex they start to fan out. Finding these lateral projections is more difficult. Finally the CA is a difficult to reconstruct tract. Due to its very thin body it is hard to find fibers that run the entire way from right to left temporal lobe. The CA is one of the tracts with the lowest performance of all methods.

As can be seen in Figure 7, the *Proposed* method yielded adequate reconstructions on all three tracts. *Multi-Mask* registration also produced convincing results on all tracts. *Atlas* registration results looked convincing on the 3D image but included segments passing gray matter and also exiting the brain mask, which is obviously wrong. *RecoBundles* showed good results for the IFO but did not manage to completely reconstruct the CA while oversegmenting the CST to neighboring gyri. *TractQuerier* did not properly segment any of the example tracts. As it defines tracts mainly by their endpoints it leaves much room for wrong turns between start and end point. Especially when using probabilistic tracking *TractQuerier* extracts a lot of false positives. The CA can not be reconstructed properly at all with *TractQuerier* as the default Freesurfer parcellation is not precise enough for the small parts of the CA. *TRACULA* yielded a good reconstruction of the stem of the CST, but missed the lateral projections. CA and IFO are not supported by *TRACULA*. *WhiteMatterAnalysis* (WMA) showed good results for the IFO but kept a lot of false positives in the CA and CST.

In a similar comparison of results on Clinical Quality dataset (figure 8), as expected, all approaches yielded segmentations of, to a varying degree, lower quality compared to the respective segmentation on the *HCP Quality* data, as can be appreciated in figure 8. The registration based approaches tended to also segment gray matter or regions outside of the brain while the streamline based approaches suffered from an increased number of false positives. *TractSeg* seems to be less affected by the lower image quality as most of the benchmark methods, as already shown by the quantitative analysis.

In general, it can be noticed that tracts tend to look well on 3D image while they show significant shortcomings on a detailed 2D image. Unfortunately, many of the relevant publications only show qualitative results using single 3D images. The segmentations of all methods and all tracts of this subject are available online³.

³ <https://doi.org/10.5281/zenodo.1154877>

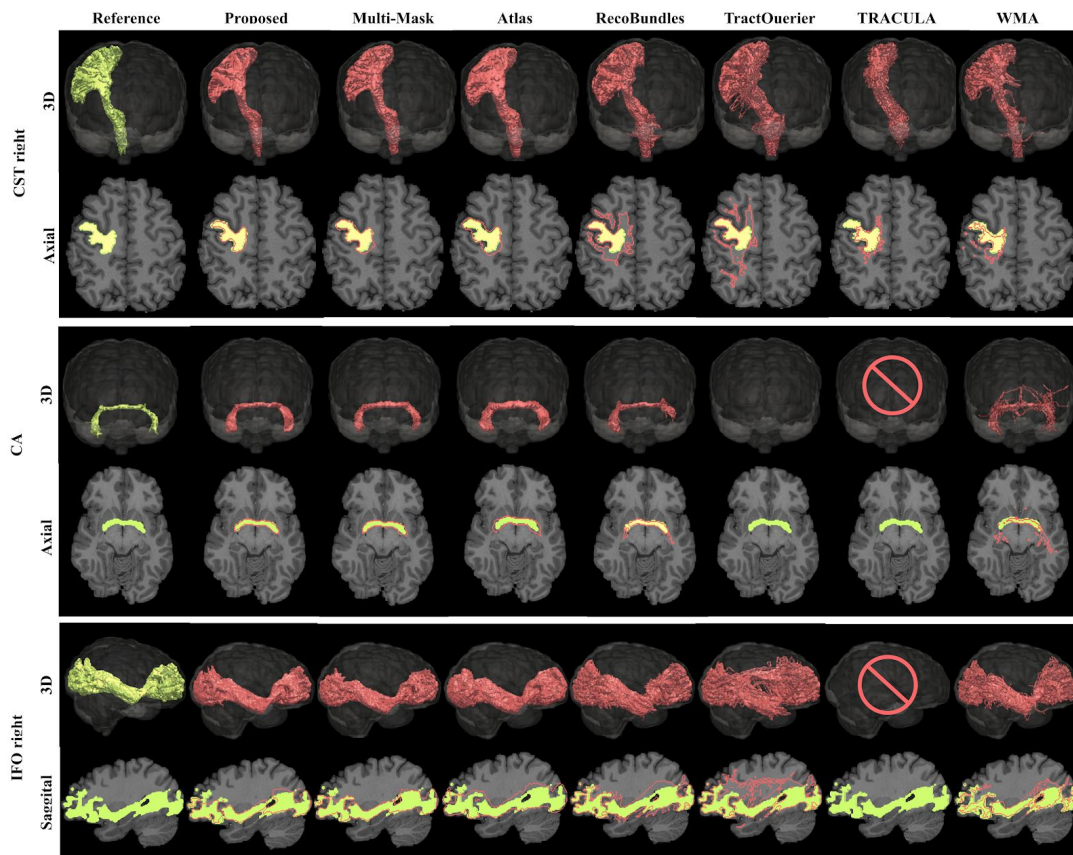


Figure 7: Qualitative comparison of results on *HCP Quality* test set: reconstruction of right corticospinal tract (CST), commissure anterior (CA) and right inferior occipito-frontal fascicle (IFO) on one random subject. *Green* shows the reference tract and *Red* the segmentation of the respective method.

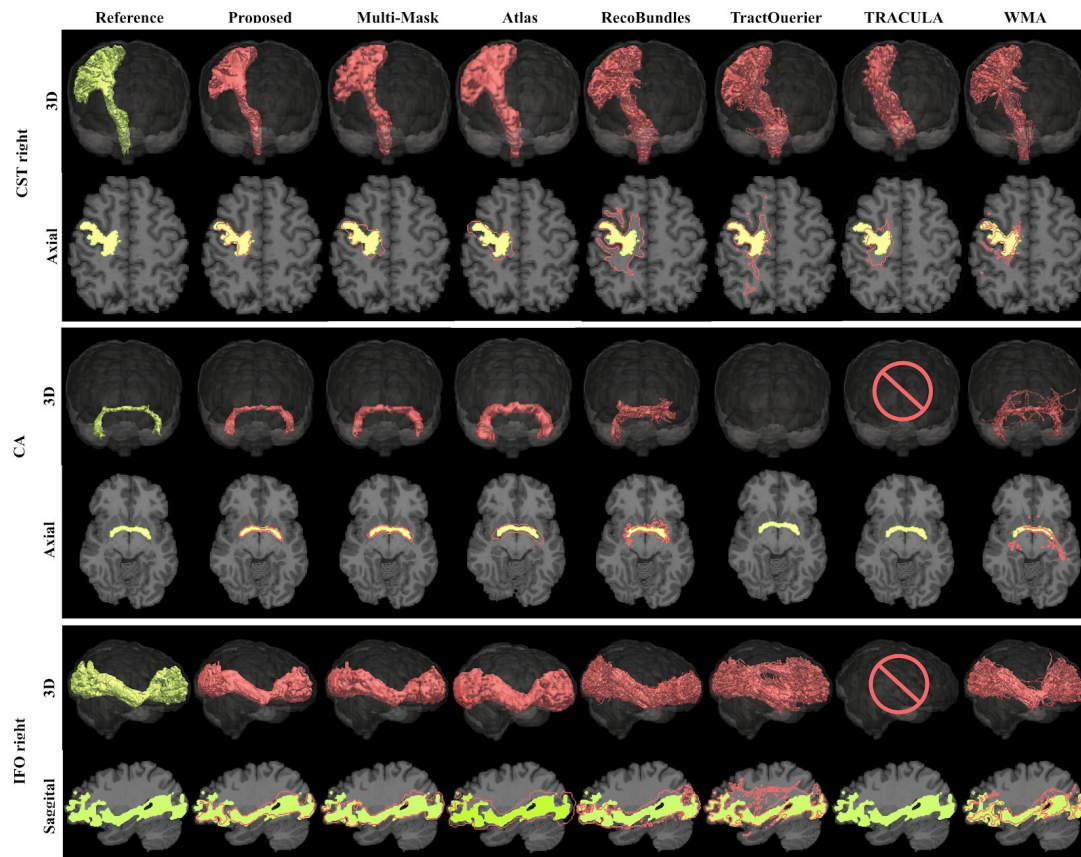


Figure 8:
 Qualitative comparison of results on *Clinical Quality* test set: reconstruction of right corticospinal tract (CST), commissure anterior (CA) and right inferior occipito-frontal fascicle (IFO) on one random subject. *Green* shows the reference tract and *Red* the segmentation of the respective method.

In some of the reference subjects some of the more difficult tracts, such as the CA and the lateral projections of the CST, were incompletely reconstructed. The original tractogram contained some sparse fibers for those regions, indicating the presence of the tract, however, when applying further constraints (ending in the correct cortex regions, angular threshold, fiber density) those sparse fibers were completely removed. Despite this noise in the training data, the proposed method managed to learn a complete representation of each tract. This enabled our model to completely segment these tracts even on subjects where the reference tracts are incomplete (see figure 9).

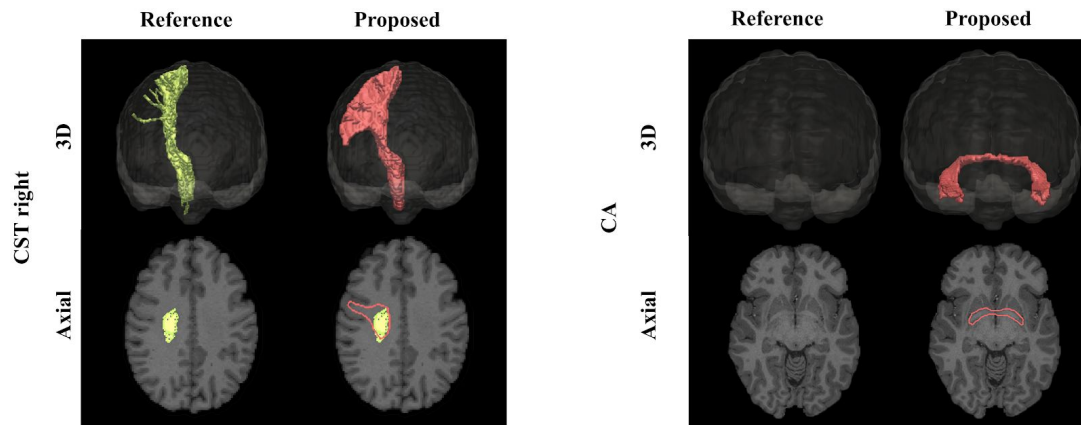


Figure 9: The proposed method creates anatomically reasonable segmentations even on subjects where the reference segmentations are incomplete due to limitations in the extraction pipeline. The presented examples are from the *Clinical Quality* dataset (subjects 979984 and 959574).

3.3. Transferability between scanners and acquisition settings

Even though trained on HCP data, TractSeg might also be able to generalize to non-HCP data. To test this capability, we applied TractSeg to four differently acquired datasets (see table 1 for an overview of the corresponding acquisition settings). The datasets contained two acquisitions from healthy probands, one provided by the TRACED challenge⁴ and one from an in-house cohort of healthy adults. The datasets further contained two patients, one schizophrenia patient from the NMorphCH project⁵ and one from an in-house cohort of patients with neurological soft signs (Hirjak et al., 2017). Figure 10 shows a selection of the obtained TractSeg segmentations (one random subject each).

Table 1: Acquisition parameters of additional non-HCP test datasets.

⁴ <https://my.vanderbilt.edu/ismrmtraced2017/>

⁵ <https://nunda.northwestern.edu/nunda/data/projects/NMorphCH>

Name	Resolution (isotrop)	Gradient shells	Preprocessing	Scanner Field Strength
TRACED	2.5mm	3x $b=0\text{mm/s}^2$, 20x $b=1000\text{mm/s}^2$, 48x $b=2000\text{mm/s}^2$, 64x $b=3000\text{mm/s}^2$	Eddy current and motion correction, denoising	3T
Internal (pathology)	2.5mm	1x $b=0\text{mm/s}^2$, 81x $b=1000\text{mm/s}^2$, 81x $b=3000\text{mm/s}^2$ (not used)	None	3T
NMorphCH	2mm	5x $b=0\text{mm/s}^2$, 30x $b=800\text{mm/s}^2$	Eddy current and motion correction, denoising	3T
Internal (healthy)	2.5mm	1x $b=0\text{mm/s}^2$, 81x $b=1000\text{mm/s}^2$, 81x $b=2000\text{mm/s}^2$, 81x $b=3000\text{mm/s}^2$,	Denoising	3T

No reference tracts are available for these datasets, so performance could only be assessed qualitatively. TractSeg yielded reasonable segmentations of the IFO on all datasets and of the CST on all datasets except for *Internal (healthy)*, where the cranial parts were not completely found. The CA was segmented completely in *TRACED*, but only fractional in the other datasets.

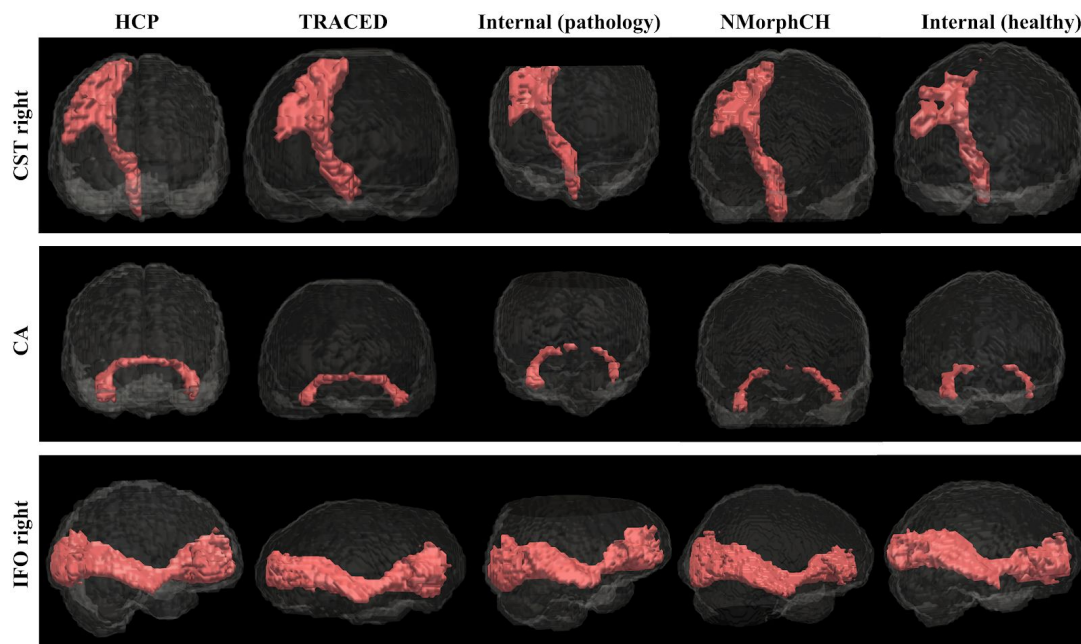


Figure 10: TractSeg segmentations on different acquisition sequences and different scanners. The results provide some initial evidence that TractSeg is able to generalize beyond the HCP data that it is currently trained on.

3.3. Fusion strategies

As described in section 2 we ran our model once for each orientation (axial, sagittal and coronal). This results in 3 predictions for each test image, which was merged into one final segmentation using a second FCNN. However, using two FCNNs instead of only one requires more resources during training and increases the runtime for inference. Therefore also two simpler fusion strategies were evaluated: Taking the *Mean* and *Majority Voting* instead of running the *Second FCNN*.

Figure 11 shows the results: *Mean* worked slightly better ($p < 0.001$) than *Majority Voting*. On *HCP Quality* *Mean* even worked slightly better ($p < 0.001$) than the *Second FCNN* approach (0.2 Dice points). However, on *Clinical Quality* *Mean* performed significantly worse ($p < 0.001$) than the *Second FCNN* (1.9 Dice points). Thus, in practical applications, the benefits of a better training and inference performance of the *Mean* fusion strategy might outweigh the gains in performance achieved by the *Second FCNN*.

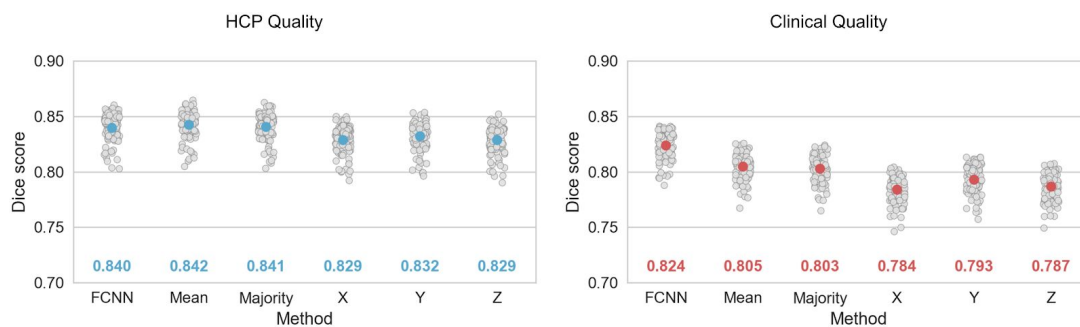


Figure 11: Results of different fusion strategies: *FCNN*: Second FCNN that receives predictions from 3 slice directions as input and produces the final output; *Mean*: Taking the mean; *Majority*: Majority voting; *X,Y,Z*: No fusion, only the respective slice direction.

Results show the mean Dice score over all tracts. Each subject is represented by one gray dot. The mean over all subjects is shown by the colored dot and the colored number.

Figure 12 shows the results of the different fusion strategies for all 72 tracts on the *Clinical Quality* dataset. *Second FCNN* consistently outperforms the simpler *Mean* fusion strategy, especially on the FX. From the single directions *Y* constantly performs better than *X* or *Z*.

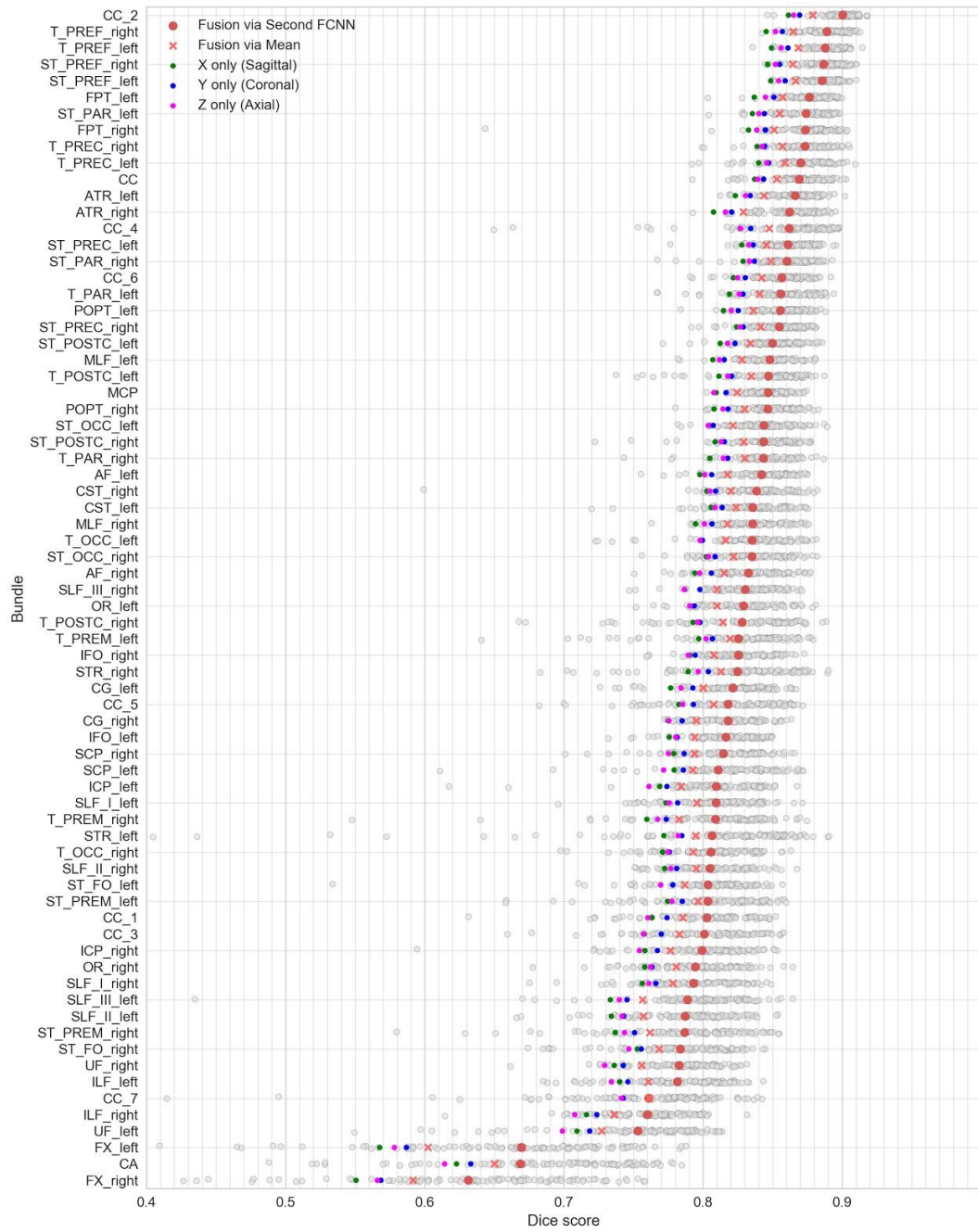


Figure 12: Mean dice scores over all subjects for 72 tracts on the *Clinical Quality* datasets using different fusion strategies (sorted by score). Gray dots show dice scores of the *Second FCNN* fusion strategy for each subject. The full name of each tract can be seen in figure 3.

3.6. Runtime

Runtime experiments were performed using a server with 48 2GHz Intel Xeon cores or an NVIDIA Titan X for the GPU-based approaches (TRACULA and our proposed method). Table 2 shows the results for each method for segmenting all tracts in a previously unseen subject. On average our method was 81x faster than the reference methods on *HCP Quality* and 535x faster on *Clinical Quality*.

Multi-Mask and *Atlas* were not included in the table since they only served as simple baseline estimation and are not openly available. Runtimes were 10.4 / 3.5 minutes (*HCP Quality* / *Clinical Quality*) and 3 / 0.4 minutes respectively.

RecoBundles, *TractQuerier* and *WhiteMatterAnalysis* showed runtimes above 950 minutes as they depend on tractography, so all the following processing steps had to be performed on thousands of streamlines. *TractQuerier* and *TRACULA* also need a cortical Freesurfer parcellation, which runs several hours.

For TractSeg, the processing step with the longest runtime was the peak extraction using the CSD, which was responsible for about 95% of the complete processing time (*HCP Quality*). The segmentation itself was quite fast with about 1 minute (with *Mean* fusion only 0.5min). We employed single-shell CSD (without multi-shell multi-tissue feature) on the *Clinical Quality* datasets, as only one shell is available here. This significantly decreased the computational burden and caused much shorter runtimes of the proposed method on lower quality data.

Table 2: Runtime in minutes for segmenting all tracts (supported by the respective method) in a new subject using the respective method.

	HCP Quality	Clinical Quality
Proposed	20.1	2.2
RecoBundles (Garyfallidis et al., 2017)	1831	1811
TractQuerier (Wassermann et al., 2016)	1704	956
WhiteMatterAnalysis (O'Donnell et al., 2012)	1052	1042
TRACULA (Yendiki et al., 2011)	1936	910

3.7. Binary mask to tractogram

TractSeg only generates binary tract masks. Should streamlines be needed, those masks make it easy to generate streamlines for a certain tract. Seeding only inside of the mask and discarding all fibers leaving the mask results in nice tract delineations as can be seen in figure 13.

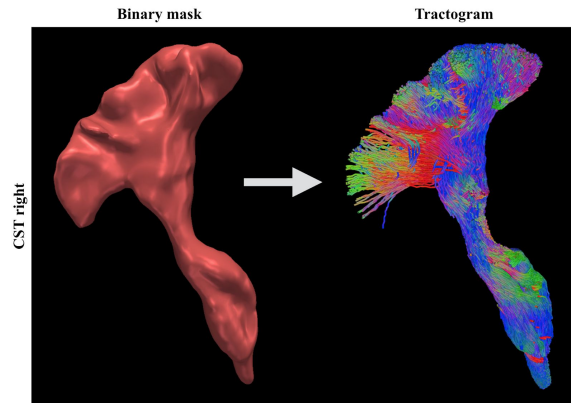


Figure 13: Using the binary mask generated by TractSeg to delineate the CST. Only fibers which never leave the mask and end in either the cortex or the brain stem were kept.

4. Discussion and Conclusion

4.1. Overview

TractSeg is a novel direct white matter tract segmentation method based on encoder-decoder FCNNs with various advantages over existing diffusion-weighted MR analysis pipelines. It was evaluated by segmenting a total of 72 tracts in a cohort of 105 HCP subjects in original high quality but also on reduced quality more clinical-like datasets. Six tract segmentation methods were used as a benchmark. Our experiments demonstrate that TractSeg achieves yet unprecedented accuracy while being less affected by the reduction in resolution on the clinical quality data.

4.2. Reference data

Regarding the reference data, although we applied extensive efforts to mitigate the limitations of tractography, our tracts do not represent a real *ground truth*. A certain amount of false positives is still remaining and for difficult to reconstruct parts like the CA or the lateral projections of the CST reconstructions are incomplete in some of the subjects (see section 3.2). Moreover the reference tracts are subject to slight variations in the detailed anatomical definition of tracts, e.g. when it comes to exact start and end regions. Despite these limitations, to the best of our knowledge, the employed data set represents one of the best existing in-vivo approximations of known white matter anatomy in a cohort of that size. Moreover, as shown section 3.2 TractSeg can handle noisy training data well, producing accurate results, even for subjects with incomplete reference tracts.

4.3. Reference methods

Selecting appropriate reference methods for a fair comparison was not easy as all methods have slightly different approaches and requirements. The comparison to our selected reference methods is also subject to some limitations:

TractQuerier was used both during the creation of the reference and during validation, inducing a potential positive bias for the method.

WMA evaluation was only available for 11 out of 20 tracts, which is not necessarily comparable. The margin between WMA and the proposed method remains, though, when restricting to these same 11

tracts. Moreover the mapping of clusters to anatomical tracts did not completely align with our reference tracts, as the finite set of distinct clusters offered by the atlas inherently limits a precise mapping. Because of the huge memory requirements of WMA for 10 million streamlines (>100GB) we had to restrict the analysis for WMA to 500k streamlines, requiring approx. 30GB of memory. This also benefited the quality of the results as cleaner clusters were created by WMA.

For RecoBundles we were only able to use 5 reference subjects due to the long runtime of RecoBundles. Using all 63 training subjects would be computationally infeasible for 72 tracts and tractograms with 10 million streamlines. Moreover, as suggested by our *Atlas* and *Multi-Mask* experiments, averaging more subjects, does not necessarily increase accuracy as small details get blurred. Therefore using 5 reference subjects provides a good estimation of the performance of RecoBundles.

TRACULA uses its own tract definitions which might differ from our definitions to some degree, introducing a negative bias. However, for very well defined tracts like the CST this bias is minor and meaningful comparison still possible.

Our results suggested that clustering based approaches (*WMA*, *RecoBundles*) perform better than *TractQuerier*, which is in line with the findings of Zhang et al. (2017).

It is interesting that the straight forward *MultiMask* method resulted in significantly better result than the more sophisticated *RecoBundles*. Both used 5 reference subjects and were based on the reference tracts, avoiding any bias induced by different tract definitions. As *RecoBundles* works in streamline space it has to deal with the large number of false positives. Clustering helps to remove the majority of those, but not all. Moreover, we used the default *RecoBundles* settings. Optimising those might improve the results to some degree.

As we have shown comparison to the reference methods has some limitations. However, those limitations alone can not explain the large accuracy gap between our method and all reference methods, indicating a strong potential of TractSeg.

4.5. Fusion of orientations

The high robustness of TractSeg towards the resolution is probably due to the heavy data augmentation, the ensembling of multiple views and the general ability of CNNs to handle noisy data well. We evaluated three different strategies to fuse the three predictions of our network for axial, sagittal and coronal input slices: Aggregation by *Mean*, aggregation by *Majority Voting* and training a *Second FCNN* to aggregate the three predictions into one final one. On the *Clinical Quality* data our *Second FCNN* approach showed a clear performance increase over the *Mean* approach, especially on the more difficult tracts (FX, CA). This confirms our assumption that a more complex fusion model can extract additional information from the different orientations. A 3D FCNN architecture would make those fusion methods obsolete, but requires more memory which made us opt for a 2D architecture. Further research in the direction of 3D architectures might be promising however.

4.6. Supervised Learning

TractSeg is based on supervised learning, bearing the inherent limitation of depending on the availability and quality of training data. This is similar to *RecoBundles*, *WMA*, *Atlas*, *MultiMask* and *TRACULA* which also require reference tracts or atlases.

Moreover TractSeg can only be applied on subjects with the same tract anatomy as the training subjects. If the tract anatomy is distorted by e.g. tumors the presented approach is not applicable

anymore. However, if training data of subject with tumors is provided TractSeg can learn to work with distorted tract anatomy.

Using scanners and acquisition sequences different from the training data introduces a domain shift, reducing performance. By using heavy data augmentation during training, our method generalizes well to datasets from other scanners and acquisition sequences, even if only trained on HCP data. We tested our method on 4 non-HCP datasets and showed promising, yet not perfect results. Further evaluation on non-HCP datasets is needed and integrating techniques for improvement of generalizability such as domain adaptation can potentially further improve the results. This will be part of our future research.

4.7. Complex pipelines

Most existing pipelines are based on several steps. For example TractQuerier first needs to perform streamline tracking, then cortical parcellation and finally the actual querying. All of those steps come with their own pitfalls and inaccuracies which accumulate further down the pipeline. Moreover, all of these steps require additional runtime and additional tools to be installed and set up. Our approach enables us to avoid steps such as atlas registration, tractography or parcellation, thereby circumventing many of the pitfalls introduced by those steps, resulting in higher accuracy, shorter runtime and easier setup. Only for generating the training data a complex pipeline was required.

4.8. Code and data availability

We are planning to make our dataset of 72 high quality tract dissections for 105 HCP subjects openly available. So far the majority of papers used their own raters to extract reference tracts. This makes meaningful comparison between methods impossible. We hope that this dataset can also help to standardize method evaluation. The first 10 subjects are available at <https://doi.org/10.5281/zenodo.1088277>. More will follow upon acceptance of this paper. TractSeg is openly available as an easy to use python package with pretrained weights: <https://github.com/MIC-DKFZ/TractSeg/>

Acknowledgments

Data were provided in part by the Human Connectome Project, WU-Minn Consortium (Principal Investigators: David Van Essen and Kamil Ugurbil; 1U54MH091657) funded by the 16 NIH Institutes and Centers that support the NIH Blueprint for Neuroscience Research; and by the McDonnell Center for Systems Neuroscience at Washington University.

This work was supported by the German Research Foundation (DFG) grant MA 6340/10-1 and grant MA 6340/12-1.

References

Avants, B.B., Epstein, C.L., Grossman, M., Gee, J.C., 2008. Symmetric diffeomorphic image registration with cross-correlation: evaluating automated labeling of elderly and neurodegenerative brain. *Med. Image Anal.* 12, 26–41. <https://doi.org/10.1016/j.media.2007.06.004>

Bazin, P.-L., Ye, C., Bogovic, J.A., Shiee, N., Reich, D.S., Prince, J.L., Pham, D.L., 2011. Direct Segmentation of the Major White Matter Tracts in Diffusion Tensor Images. *NeuroImage* 58, 458–468. <https://doi.org/10.1016/j.neuroimage.2011.06.020>

Bells, S., Cercignani, M., Deoni, S., Assaf, Y., Pasternak, O., Evans, C., Leemans, A., Jones, D., 2011. Tractometry—comprehensive multi-modal quantitative assessment of white matter along specific tracts. In: *Proc. ISMRM*, vol. 678.

Çiçek, Ö., Abdulkadir, A., Lienkamp, S.S., Brox, T., Ronneberger, O., 2016. 3D U-Net: Learning Dense Volumetric Segmentation from Sparse Annotation, in: *Medical Image Computing and Computer-Assisted Intervention – MICCAI 2016, Lecture Notes in Computer Science*. Presented at the International Conference on Medical Image Computing and Computer-Assisted Intervention, Springer, Cham, pp. 424–432. https://doi.org/10.1007/978-3-319-46723-8_49

Clayden, J.D., Storkey, A.J., Bastin, M.E., 2007. A Probabilistic Model-Based Approach to Consistent White Matter Tract Segmentation. *IEEE Transactions on Medical Imaging* 26, 1555–1561. <https://doi.org/10.1109/TMI.2007.905826>

Clayden, J.D., Storkey, A.J., Maniega, S.M., Bastin, M.E., 2009. Reproducibility of tract segmentation between sessions using an unsupervised modelling-based approach. *NeuroImage* 45, 377–385. <https://doi.org/10.1016/j.neuroimage.2008.12.010>

Cook, P.A., Zhang, H., Avants, B.B., Yushkevich, P., Alexander, D.C., Gee, J.C., Ciccarelli, O., Thompson, A.J., 2005. An Automated Approach to Connectivity-Based Partitioning of Brain Structures, in: *Medical Image Computing and Computer-Assisted Intervention – MICCAI 2005, Lecture Notes in Computer Science*. Presented at the International Conference on Medical Image Computing and Computer-Assisted Intervention, Springer, Berlin, Heidelberg, pp. 164–171. https://doi.org/10.1007/11566465_21

Dayan, M., Monohan, E., Pandya, S., Kuceyeski, A., Nguyen, T.D., Raj, A., Gauthier, S.A., 2016. Profilmetry: a new statistical framework for the characterization of white matter pathways, with application to multiple sclerosis. *Hum. Brain Mapp.* 37 (3), 989–1004.

Dieleman, S., Schlüter, J., Raffel, C., Olson, E., Sønderby, S.K., Nouri, D., Maturana, D., Thoma, M., Battenberg, E., Kelly, J., Fauw, J.D., Heilman, M., Almeida, D.M. de, McFee, B., Weideman, H., Takács, G., Rivaz, P. de, Crall, J., Sanders, G., Rasul, K., Liu, C., French, G., Degraeve, J., 2015. Lasagne: First release. <https://doi.org/10.5281/zenodo.27878>

Dumoulin V., Visin F., 2016. A guide to convolution arithmetic for deep learning. *ArXiv160307285 Stat.*

Eckstein, I., Shattuck, D.W., Stein, J.L., McMahon, K.L., de Zubicaray, G., Wright, M.J., Thompson, P.M., Toga, A.W., 2009. Active fibers: matching deformable tract templates to diffusion tensor images. *NeuroImage* 47 Suppl 2, T82-89. <https://doi.org/10.1016/j.neuroimage.2009.01.065>

Garyfallidis, E., Brett, M., Correia, M.M., Williams, G.B., Nimmo-Smith, I., 2012. QuickBundles, a Method for Tractography Simplification. *Front. Neurosci.* 6. <https://doi.org/10.3389/fnins.2012.00175>

- Garyfallidis, E., Côté, M.-A., Rheault, F., Sidhu, J., Hau, J., Petit, L., Fortin, D., Cunanne, S., Descoteaux, M., 2017. Recognition of white matter bundles using local and global streamline-based registration and clustering. *NeuroImage*. <https://doi.org/10.1016/j.neuroimage.2017.07.015>
- Hernández, M., Guerrero, G.D., Cecilia, J.M., García, J.M., Inuggi, A., Jbabdi, S., Behrens, T.E.J., Sotiropoulos, S.N., 2013. Accelerating Fibre Orientation Estimation from Diffusion Weighted Magnetic Resonance Imaging Using GPUs. *PLOS ONE* 8, e61892. <https://doi.org/10.1371/journal.pone.0061892>
- Hirjak, D., Thomann, P.A., Wolf, R.C., Kubera, K.M., Goch, C., Hering, J., Maier-Hein, K.H., 2017. White matter microstructure variations contribute to neurological soft signs in healthy adults. *Hum. Brain Mapp*. <https://doi.org/10.1002/hbm.23609>
- Jeurissen, B., Tournier, J.-D., Dhollander, T., Connelly, A., Sijbers, J., 2014. Multi-tissue constrained spherical deconvolution for improved analysis of multi-shell diffusion MRI data. *NeuroImage* 103, 411–426. <https://doi.org/10.1016/j.neuroimage.2014.07.061>
- Jin, Y., Shi, Y., Zhan, L., Gutman, B.A., de Zubicaray, G.I., McMahon, K.L., Wright, M.J., Toga, A.W., Thompson, P.M., 2014. Automatic clustering of white matter fibers in brain diffusion MRI with an application to genetics. *NeuroImage* 100, 75–90. <https://doi.org/10.1016/j.neuroimage.2014.04.048>
- Kingma, D.P., Ba, J., 2014. Adam: A Method for Stochastic Optimization. *ArXiv14126980 Cs*.
- Labra, N., Guevara, P., Duclap, D., Houenou, J., Poupon, C., Mangin, J.-F., Figuerola, M., 2017. Fast Automatic Segmentation of White Matter Streamlines Based on a Multi-Subject Bundle Atlas. *Neuroinform* 15, 71–86. <https://doi.org/10.1007/s12021-016-9316-7>
- Lenglet, C., Rousson, M., Deriche, R., 2006. DTI segmentation by statistical surface evolution. *IEEE Trans. Med. Imaging* 25, 685–700.
- Maier-Hein, K.H., Neher, P.F., Houde, J.-C., Côté, M.-A., Garyfallidis, E., Zhong, J., Chamberland, M., Yeh, F.-C., Lin, Y.-C., Ji, Q., Reddick, W.E., Glass, J.O., Chen, D.Q., Feng, Y., Gao, C., Wu, Y., Ma, J., Renjie, H., Li, Q., Westin, C.-F., Deslauriers-Gauthier, S., González, J.O.O., Paquette, M., St-Jean, S., Girard, G., Rheault, F., Sidhu, J., Tax, C.M.W., Guo, F., Mesri, H.Y., Dávid, S., Froeling, M., Heemskerk, A.M., Leemans, A., Boré, A., Pinsard, B., Bedetti, C., Desrosiers, M., Brambati, S., Doyon, J., Sarica, A., Vasta, R., Cerasa, A., Quattrone, A., Yeatman, J., Khan, A.R., Hodges, W., Alexander, S., Romascano, D., Barakovic, M., Auria, A., Esteban, O., Lemkaddem, A., Thiran, J.-P., Cetingul, H.E., Odry, B.L., Mailhe, B., Nadar, M.S., Pizzagalli, F., Prasad, G., Villalon-Reina, J.E., Galvis, J., Thompson, P.M., Requejo, F.D.S., Laguna, P.L., Lacerda, L.M., Barrett, R., Dell'Acqua, F., Catani, M., Petit, L., Caruyer, E., Daducci, A., Dyrby, T.B., Holland-Letz, T., Hilgetag, C.C., Stieltjes, B., Descoteaux, M., 2017. The challenge of mapping the human connectome based on diffusion tractography. *Nature Communications* 8, 1349. <https://doi.org/10.1038/s41467-017-01285-x>
- Nair, V., Hinton, G., 2010. Rectified Linear Units Improve Restricted Boltzmann Machines. *ICML*.

O'Donnell, L.J., Suter, Y., Rigolo, L., Kahali, P., Zhang, F., Norton, I., Albi, A., Olubiyi, O., Meola, A., Essayed, W.I., Unadkat, P., Ciris, P.A., Wells, W.M., Rathi, Y., Westin, C.-F., Golby, A.J., 2016. Automated white matter fiber tract identification in patients with brain tumors. *NeuroImage Clin.* 13, 138–153. <https://doi.org/10.1016/j.nicl.2016.11.023>

O'Donnell, L.J., Wells, W.M., Golby, A.J., Westin, C.-F., 2012. Unbiased groupwise registration of white matter tractography. *Med. Image Comput. Comput.-Assist. Interv. MICCAI Int. Conf. Med. Image Comput. Comput.-Assist. Interv.* 15, 123–130.

O'Donnell, L.J., Westin, C.-F., 2007. Automatic tractography segmentation using a high-dimensional white matter atlas. *IEEE Trans. Med. Imaging* 26, 1562–1575. <https://doi.org/10.1109/TMI.2007.906785>

Pujol, S., Wells, W., Pierpaoli, C., Brun, C., Gee, J., Cheng, G., Vemuri, B., Commowick, O., Prima, S., Stamm, A., Goubran, M., Khan, A., Peters, T., Neher, P., Maier-Hein, K.H., Shi, Y., Tristan-Vega, A., Veni, G., Whitaker, R., Styner, M., Westin, C.-F., Gouttard, S., Norton, I., Chauvin, L., Mamata, H., Gerig, G., Nabavi, A., Golby, A., Kikinis, R., 2015. The DTI Challenge: Toward Standardized Evaluation of Diffusion Tensor Imaging Tractography for Neurosurgery. *J. Neuroimaging Off. J. Am. Soc. Neuroimaging* 25, 875–882. <https://doi.org/10.1111/jon.12283>

Ratnarajah, N., Qiu, A., 2014. Multi-label segmentation of white matter structures: application to neonatal brains. *NeuroImage* 102 Pt 2, 913–922. <https://doi.org/10.1016/j.neuroimage.2014.08.001>

Ronneberger, O., Fischer, P., Brox, T., 2015. U-Net: Convolutional Networks for Biomedical Image Segmentation. *ArXiv150504597 Cs*.

Siless, V., Chang, K., Fischl, B., Yendiki, A., 2018. Anatomical Cuts: Hierarchical clustering of tractography streamlines based on anatomical similarity. *NeuroImage* 166, 32–45. <https://doi.org/10.1016/j.neuroimage.2017.10.058>

Sotiropoulos, S.N., Jbabdi, S., Xu, J., Andersson, J.L., Moeller, S., Auerbach, E.J., Glasser, M.F., Hernandez, M., Sapiro, G., Jenkinson, M., Feinberg, D.A., Yacoub, E., Lenglet, C., Van Essen, D.C., Ugurbil, K., Behrens, T.E.J., 2013. Advances in diffusion MRI acquisition and processing in the Human Connectome Project. *NeuroImage, Mapping the Connectome* 80, 125–143. <https://doi.org/10.1016/j.neuroimage.2013.05.057>

Srivastava, N., Hinton, G.E., Krizhevsky, A., Sutskever, I., Salakhutdinov, R., 2014. Dropout: a simple way to prevent neural networks from overfitting. *J. Mach. Learn. Res.* 15, 1929–1958.

Stieltjes, B., Brunner, R., Maier-Hein, K., Laun, F., 2013. Diffusion tensor imaging: introduction and atlas.

Thiebaut de Schotten, M., ffytche, D.H., Bizzi, A., Dell'Acqua, F., Allin, M., Walshe, M., Murray, R., Williams, S.C., Murphy, D.G.M., Catani, M., 2011. Atlasing location, asymmetry and inter-subject

variability of white matter tracts in the human brain with MR diffusion tractography. *NeuroImage* 54, 49–59. <https://doi.org/10.1016/j.neuroimage.2010.07.055>

Tournier, J.-D., Calamante, F., Connelly, A., 2010. Improved probabilistic streamlines tractography by 2nd order integration over fibre orientation distributions. *Proc Intl Soc Mag Reson Med ISMRM* 18.

Tournier, J.-D., Calamante, F., Connelly, A., 2007. Robust determination of the fibre orientation distribution in diffusion MRI: non-negativity constrained super-resolved spherical deconvolution. *NeuroImage* 35, 1459–1472. <https://doi.org/10.1016/j.neuroimage.2007.02.016>

Van Essen, D.C., Smith, S.M., Barch, D.M., Behrens, T.E.J., Yacoub, E., Ugurbil, K., 2013. The WU-Minn Human Connectome Project: An overview. *NeuroImage, Mapping the Connectome* 80, 62–79. <https://doi.org/10.1016/j.neuroimage.2013.05.041>

Wang, R., Benner, T., Sorensen, A.G., Wedeen, V.J., 2007. Diffusion toolkit: a software package for diffusion imaging data processing and tractography. *Proc Intl Soc Mag Reson Med* 15.

Wassermann, D., Makris, N., Rathi, Y., Shenton, M., Kikinis, R., Kubicki, M., Westin, C.-F., 2016. The white matter query language: a novel approach for describing human white matter anatomy. *Brain Struct. Funct.* 221, 4705–4721.

Wilcoxon, F., 1945. Individual Comparisons by Ranking Methods. *Biom. Bull.* 1, 80–83. <https://doi.org/10.2307/3001968>

Yeatman, J.D., Dougherty, R.F., Myall, N.J., Wandell, B.A., Feldman, H.M., 2012. Tract profiles of white matter properties: automating fiber-tract quantification. *PloS One* 7, e49790. <https://doi.org/10.1371/journal.pone.0049790>

Yendiki, A., Panneck, P., Srinivasan, P., Stevens, A., Zöllei, L., Augustinack, J., Wang, R., Salat, D., Ehrlich, S., Behrens, T., Jbabdi, S., Gollub, R., Fischl, B., 2011. Automated Probabilistic Reconstruction of White-Matter Pathways in Health and Disease Using an Atlas of the Underlying Anatomy. *Front. Neuroinformatics* 5.

Zhang, F., Norton, I., Cai, W., Song, Y., Wells, W.M., O'Donnell, L.J., 2017. Comparison between two white matter segmentation strategies: An investigation into white matter segmentation consistency, In: 2017 IEEE 14th International Symposium on Biomedical Imaging (ISBI 2017), pp. 796–799. <https://doi.org/10.1109/ISBI.2017.7950638>